A simple method for quantitative imaging of 2D acoustic fields using refracto-vibrometry

Robert Malkin[1*], Thomas Todd[2], Daniel Robert[1]

1 - School of Biological Sciences

University of Bristol, England, BS8 1TQ

2 - Complexity Sciences, Faculty of Engineering

University of Bristol, England, BS8 1TR

* corresponding author: r.e.malkin@gmail.com

Tel: +44 (0) 117 928 7484

Abstract

This paper presents a simple 2D method for rapid time resolved quantitative imaging of acoustic waves using refracto-vibrometry. We present the theoretical background, the experimental method and reconstructions of acoustic reflection and interference. We investigate the applicability of the method, in particular the effect of sound radiator geometry. Finite element and experimental reconstructions of the sound fields are analysed. The spatial limitations and accuracy of the method are presented and discussed.

Keywords:

1. Laser Doppler vibrometry
2. Refracto-vibrometry
3. Acoustic structure interaction
4. Finite element analysis

1 Introduction

Quantified reconstruction of acoustic fields is often done using microphone arrays. These arrays tend to be expensive, bulky and uncertainty arises at higher frequencies where microphones can interfere with the sound field. Non-invasive methods are also commonly employed [1]. Schlieren photography and shadowgraphy are well known methods of visualising acoustic fields but lack the ability of simple pressure field quantification [2,3]. The calculation of instantaneous sound pressure using light intensity measurements has been shown to be sensitive and accurate [4]. The use of laser Doppler vibrometry to measure pressure fluctuations has received significant attention [5–12], including tomographic 3D field reconstruction [13–17]. Previous research has shown that quantified sound field visualisation is possible but the implementation is relatively complex.

A key aspect in interpreting refracto-vibrometry data is the averaging of the pressure's spatial distribution. Effectively a 3D sound field is reduced to a 2D projection. We investigate the effect of this projection for two distinct sound radiators, a point and planar source. The quantification of the projected sound field requires knowledge of the laser path through the 3D field. Using numerical simulations we study the ability to quantify the projected field for both sources, and highlight the errors induced by a scanning vibrometer. We then apply the method for quantified visualisation of two well-known acoustic phenomena, reflection and interference.

2 Theory of refracto-vibrometry

The refractive index, *n*, of a medium is defined as;

$$n \equiv \frac{c_0}{v} \tag{1}$$

With c_0: velocity of light in a vacuum and *v*: the velocity of light in the medium. The refractive index of air is influenced by pressure, temperature, humidity and frequency (although the dispersive effect is relatively small in standard conditions) [18–20]. In a simple adiabatic system a change in pressure results in a corresponding change in *n*. The resulting changes in propagation velocity, v, can be measured using a laser Doppler vibrometer (LDV) [6,7,21]. The technique of refracto-vibrometry has primarily been used for acoustic pressure visualisation in air and water [13,21–24]. The principle of the measurement technique is described by *Nakamura et al.* [25] and is illustrated in Figure 1.

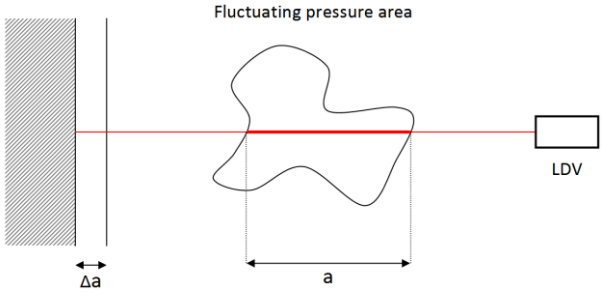

Figure 1 - Using LDV, a rigid wall (shaded structure on the left) appears to be displaced by a distance of *Δa* . This is due to the modulation of the velocity of light propagation within the fluctuating pressure area, of length *a*.

Monochromatic laser light travelling through a region of sound pressure of length *a,* results in a corresponding variation in the magnitude of *n*. The laser light exits the region and, if reflected from a rigid wall, travels back through the region and to the LDV. This modulated path appears identical to a physical displacement of the reflective rigid wall, *Δa*.

$$n \cdot \Delta a = \Delta n \cdot a \tag{2}$$

Where the apparent displacement of the rigid wall, *Δa*, is given by integrating the LDV velocity (with respect to time) output signal. It has been shown that the pressure-refraction relation may be expressed in terms of temperature, pressure and relative humidity [26]. It is formalised by the expression:

$$n = 1 + \frac{7.86 \cdot 10^{-4} \cdot P}{273 + T} - (1.50 \cdot 10^{-11}) \cdot RH(T^2 + 160) \tag{3}$$

With *P*: pressure in kPa, *T*: temperature in °C and *RH*: relative humidity in %. At 1 atmosphere of pressure, 20°C temperature and a relative humidity of 50%, Eq. 3 gives *n* a value of 1.0002714. This relation between pressure and *n* allows us to relate the (observed) apparent displacement of the rigid wall to the pressure in the region of interest. Assuming an adiabatic process,

$$\frac{\Delta n}{\Delta P} = \beta = 2.68 \cdot 10^{-9}\ per\ Pa \tag{4}$$

Combining Eq. (2) and Eq. (4);

$$\Delta P = \frac{\Delta n}{2.68 \cdot 10^{-9}} = \frac{n}{a} \cdot \frac{\Delta a}{\beta} \tag{5}$$

The method of operation requires the laser to pass through the length of the region, *a*, meaning that the resulting velocity change is the integration of the average pressure distribution along the length of the path. As the laser travels from the LDV to the reflector and back, the resulting measured velocity from the LDV is an integration along the whole path length. The pressure field is likely to be variable along this length, therefore quantification of the field using Eq. (5) is complicated as the length *a* is unknown, as detailed by Olsson & Tatar in 2006 [9] and Paone & Revel [11]. Olsson & Tatar note that "any quantitative data obtained when measuring 3D sound fields using laser vibrometry must be viewed with some scepticism" due to the line integration problem when using a point source. In 2007, however, Olsson showed that the method could be used to measure the pressure magnitude correctly by using a correction factor [27]. While the results were accurate, Olsson's method did not lend itself to simple measurement of sound fields, requiring considerable technical expertise. Zipser *et al* took the approach of using a solid glass partition as a waveguide thereby constraining the region in which the sound was propagating [22]. This approach results in accurate quantification, yet precludes the use of free field conditions.

3 Theoretical analysis of line integration of acoustic pressure

Here we use a 2D transient finite element analysis (FEA) (Comsol 4.3) model of acoustic pressure at 5, 10 & 20kHz for two acoustic radiators; a point source and a planar loudspeaker (with a width, *w*, of 150mm, equal to that of the speaker used in experiments), shown in Figure 2.

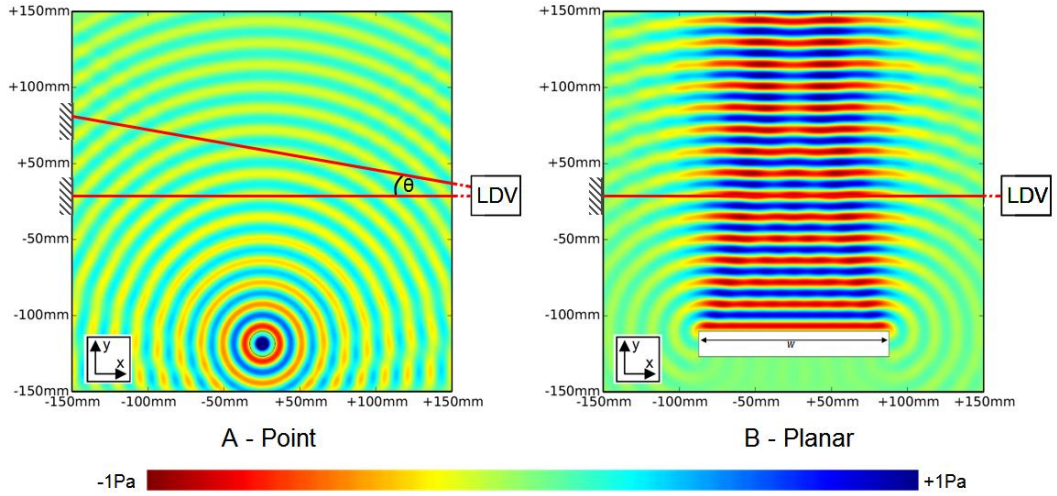

Figure 2 - Simulated instantaneous sound fields at 20kHz showing the position of the LDV and the rigid reflector (hatched area on Y-axis). A: field radiated from a point source showing the scanning angle θ, highlighting the alteration of the laser light path. B: field radiated from a planar source.

In the experimental situation, the laser scanner (Polytec PSV-400) controls the position of the laser beam using rotating mirrors. This results in scan lines that are non-parallel, fanning out from the LDV with angle θ (shown in Figure 2-A), the effect of which was commented on by Solodov *et al* [28]. For the present experimental work, the distance from the LDV to the reflecting wall (2m) was such that the maximum scanning angle was 2.6°. To investigate the effect of these non-parallel scan lines for the planar source case, the average pressure along a scan line (red line, Figure 2-B) is compared to a point measurements along the y-axis for y>0mm at x=0mm. The results of this theoretical model-based analysis at 5, 10 and 20kHz are shown in Figure 3. For the outermost scan lines, the inferred pressure value may be underestimated by as much as 15% for 20kHz. This error increases rapidly with increasing frequency as the wavelength shortens and scan lines 'traverse' an increasing number of wave fronts. For a general experimental case, this error may be reduced by: (1) increasing the distance between LDV and reflecting wall, (2) replacing the planar loudspeaker with one of narrower width, *w,* and (3) increasing the wavelength. These three optimisations can be used individually or in combination. For the FEA we assume the scan lines as to be parallel.

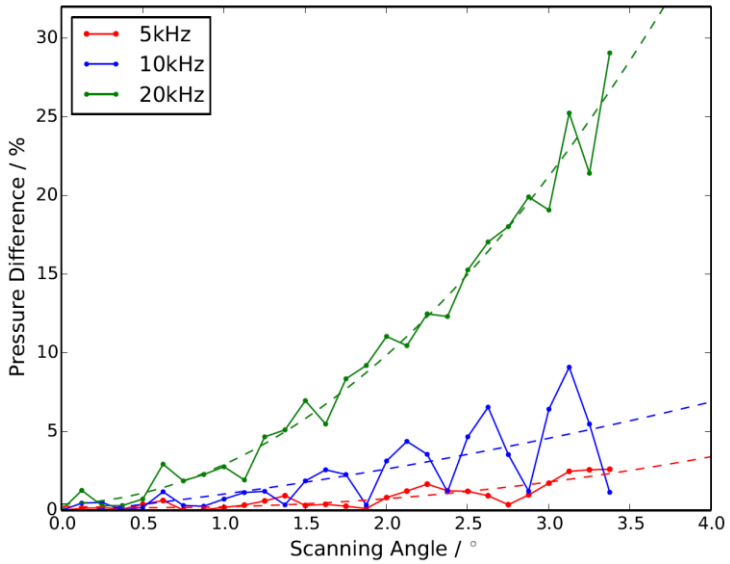

Figure 3 – Experimental data of the effect of non-parallel scan lines on actual and line averaged pressure values taken at a single phase of sound pressure. Dashed lines show polynomial fit to data.

3.1 Instantaneous and cumulative pressure

The experimental measurements provide pressure estimates that are an average along the laser path. The FEA models, however, allow us to probe the instantaneous pressure values along the line of integration, and study the phenomenon in greater detail. Simulating the line integration effect for a sound source of known geometry is useful to investigate the practicality of refracto-vibrometry for accurate measurements of pressure fields.

The instantaneous pressure value along a single scan line (example shown in Figure 2) was plotted as a function of the distance along that scan line (Figure 4-A&C). Then, the cumulative pressure value is calculated along the same scan line (Figure 4-B&D). The total cumulative pressure value, defined here as δ, is measured. In the example shown in Figure 4, $\delta \approx$-750Pa and $\delta \approx$+7,000Pa for the point and planar source, respectively. δ is in effect equivalent to the instantaneous velocity signal from the LDV. We then calculate the coordinates along the scan line where the cumulative pressure equals 0.95δ (black dots in Figure 4-B&C). The 5% is used to reduce the number of data points (black dots), simplifying the analysis without compromising accuracy. Thresholds between 0.9δ and 0.99δ gave similar results, but data were visually less accessible when overlaid onto the pressure distribution.

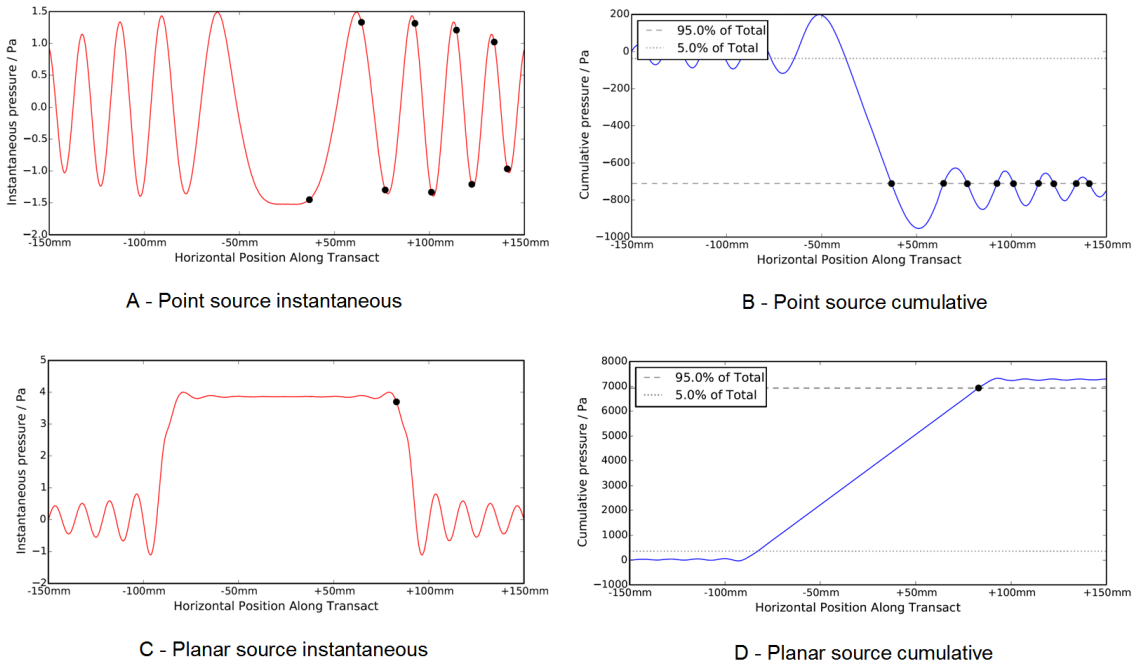

Figure 4 – Modelled instantaneous (A-C) and cumulative (B-D) pressure values for a point (A-B) and planar (C-D) radiator, as shown in Figure 2. Black dots indicate locations of equal cumulative pressure, shown only for horizontal position x>0mm.

We then map these coordinates onto the instantaneous pressure plots (Figure 4-A&C). This analytical procedure allows the measurement of the locations along the scan line that contributed to the observed average pressure. There are situations where multiple points reach the average cumulative pressure of 0.95δ. The physical interpretation is that the measured average cumulative pressure can be a contribution from several segments along the scan line, each of which have the same value of δ. This results in uncertainty about the acoustic beam width, a, which is required for quantification.

3.2 Acoustic beam width, a

We apply the method described above to 220 parallel scan lines (corresponding to 15 scan lines per wavelength at 20kHz) on the sound fields for a point and planar source at 5, 10 & 20kHz. The coordinates of the black dots are then overlaid onto the 2D pressure fields Figure 5. The spatial distribution of the black dots is also represented in a corresponding histogram. The histograms may be used to estimate the acoustic beam width, a. This is seen most clearly in the histograms for the planar source which yield two clear peaks (increasing in sharpness at higher frequency). The distance between these two peaks is used to estimate, a, thereby allowing quantification using Eq. (5). The highly scattered distribution of black dots for the point source shows no clear boundary that permits the unambiguous determination of a. The analysis highlights the limitations encountered for a single point source, namely a fluctuating value of a. The same analysis conducted at different phase angles showed the planar source width to be temporally stable.

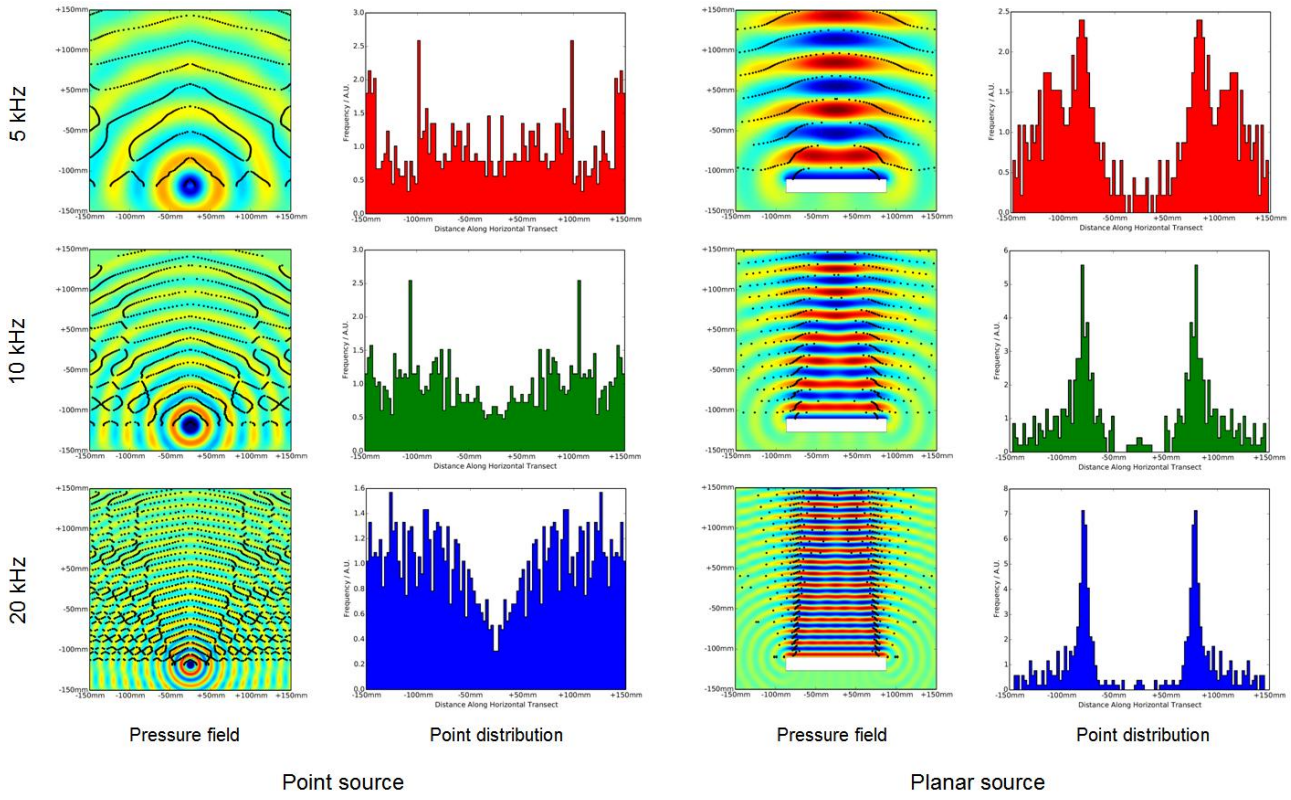

Figure 5 – Instantaneous pressure distributions for point and planar sources. Pressure fields overlaid with coordinates equal to 0.95δ and the corresponding distribution histograms. The planar source histograms show peaks defining *a*. The point source histograms illustrate the lack of a definitive value of *a*.

4 Imaging of the acoustic field

4.1 Experimental procedure

To illustrate the feasibility of the method, acoustic reflection and interference are visualised employing the analytical rationale described above.

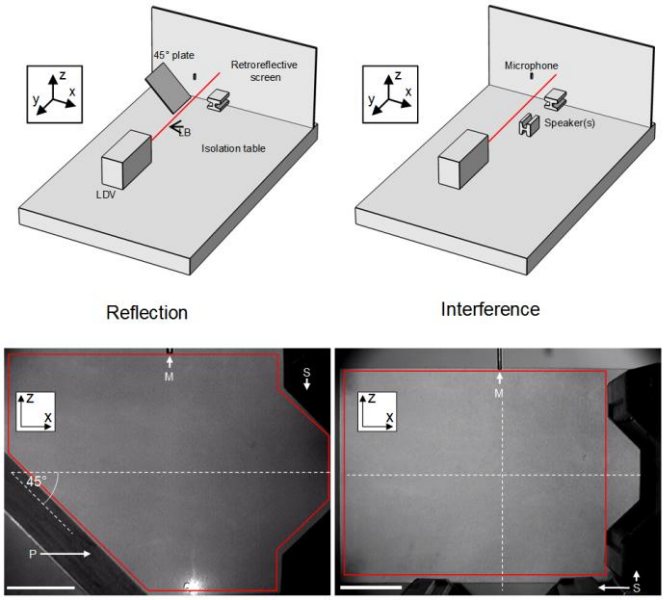

Figure 6 - Experimental setup to visualise acoustic reflection and interference. Top panels: Diagrammatic representation of components and their relative positions in experimental setup (not to scale). Bottom panels: Images from LDV showing the scanning area (outlined in red). Scale bars: 50mm. M: microphone, P: plate, S: loudspeaker, LB: laser beam.

The structure and propagation of acoustic waves were visualised for a wave packet of 5 cycles at 20kHz. Other experiments, using frequencies between 5-20kHz and other continuous tones showed similar results. Continuous tones however suffered from noisy signal from the numerous reflections within the acoustic booth used. The 5-cycles wave packet corresponds to 250µs signal duration at 20kHz, a time short enough to allow for repeat measurements (n=50) at each of the scan points, prior to the linear averaging of the velocity signal. The acoustic signal was generated by a waveform generator (Agilent 33120A), and fed to the high frequency planar loudspeakers (AMT-1, ESS laboratories). The sound radiating Mylar membrane of the planar loudspeaker had a rectangular shape of 150mm length and 5mm width. Sampling frequency of the LDV was 512kHz and spatial resolution was set at 15 measuring points per wavelength in air. At 20kHz, this corresponds to ca. 9 points per centimetre. For all measurements, a calibrated precision reference microphone (Brüel & Kjær type 4138) was placed next to the observed pressure field, using a preamplifier (Brüel & Kjær, type 2633), and power supply (Brüel & Kjær, type 5935). The microphone signal is used to provide a calibrated reference in dB sound pressure level (SPL) (re. 20µPa).

One conceivable caveat of the method is that the acoustic energy from the loudspeakers could mechanically actuate the rigid wall used as the reflector. In effect, the laser signal does not distinguish between a fluctuation of the air refractive index along the line of integration and the sound-induced motion of the reflective wall. To investigate whether the recorded signals are affected by such mixing, a loudspeaker was positioned behind the reflective wall and vibrations (which in this case should be purely mechanical) on the reflective wall were measured. At the sound pressures and frequencies used here, the mechanical displacement velocity of the wall did not exceed background noise at all frequencies considered (5-20kHz).

4.2 Imaging acoustic of reflection

The reflection experiment reveals the time-resolved evolution of the wave packet as it encounters a reflective aluminium plate of 3mm thickness. Here, a single loudspeaker was positioned such that its acoustic axis was directed towards the aluminium plate at 45° angle of incidence (Figure 6). The temporal evolution of the pressure field was measured in the space between the loudspeaker and the plate (Figure 7). Pressure values were calculated from LDV displacement values for each scanning point using Eq. (5) (with a length of a as determined in Figure 5).

For time, $0<t<3.9T$ (T: period at 20kHz), the wave packet is seen to propagate towards the aluminium plate. At $t=3.9T$ the first sign of reflection and interference become apparent. The loudspeaker's inertia results in additional oscillations visible in the wake of the initial wave packet, detectable after $t>1.3T$, and absent in the FE model. At $t=6.6T$ the wave packet is half reflected from the plate, giving rise to the interference pattern. At $t>9.2T$ the wave packet has been fully reflected at an angle of 90°.

The experimental data is in good agreement with the finite element simulation, generating near to identical patterns of constructive and destructive interference (Figure 7). There is, however, some disagreement between the measured and predicted pressure values (Figure 7, t=0.0T) very close to the loudspeaker, where the FE model predicts higher pressures than the LDV. This discrepancy is likely due to two distinct effects; (1) the measurement error introduced from the non-parallel scanning lines, and speculatively (2) this region of the acoustic field is well within the loudspeaker's near-field. The applicability of the presented method in the near-field remains unexplored to date.

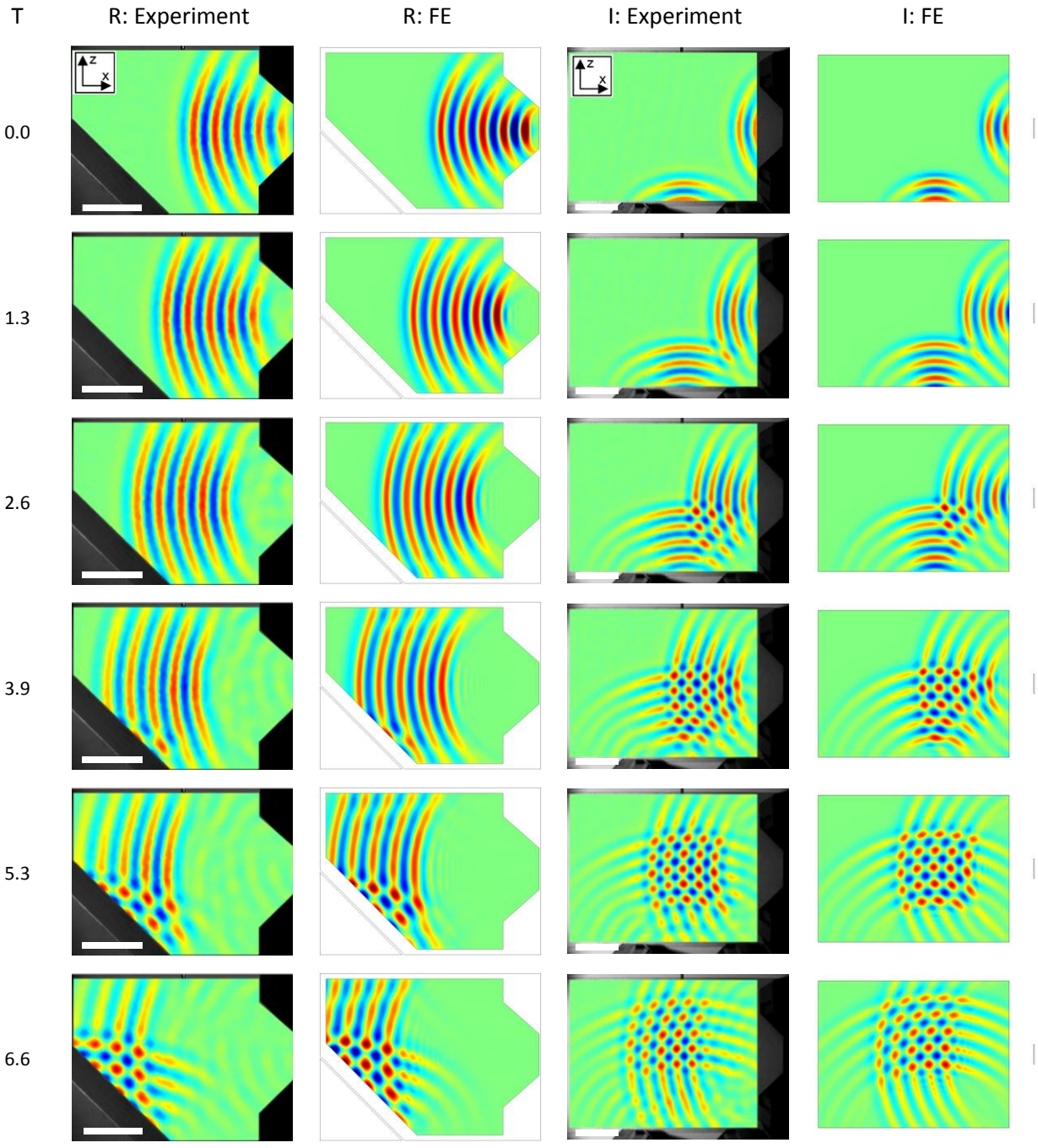

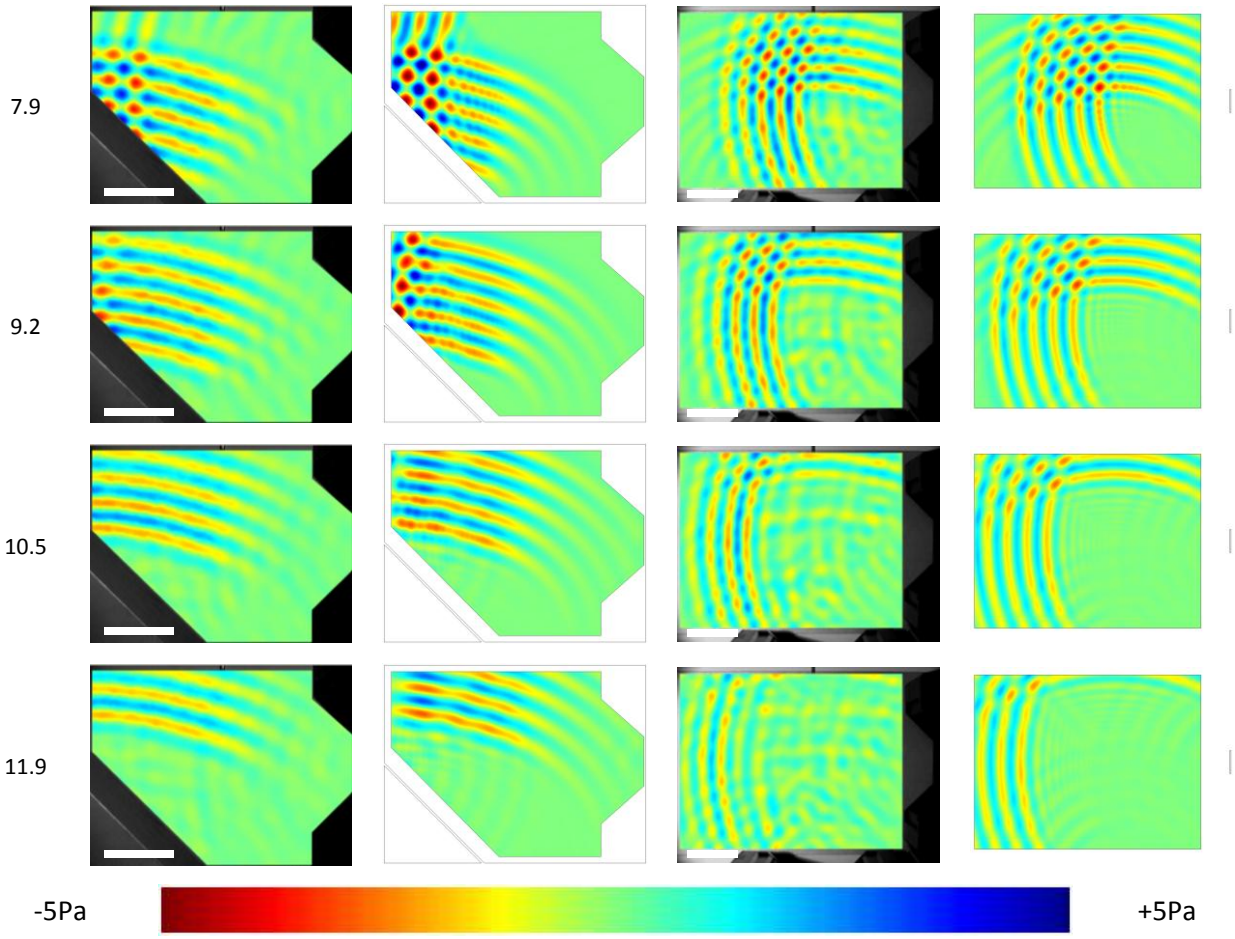

Figure 7 - Experimental and FE representations of pressure field with increasing time steps. Scale bar: 5cm. T: period (T=50µs), R: reflection, I: interference.

4.3 Imaging acoustic of interference

Acoustic interference was generated using two loudspeakers, oriented at 90° to each other (Figure 6). LDV refractometry was then used to image the temporal evolution of the sound field as the two synchronously radiated and identical wave packets interfered (Figure 7). Interference patterns begin to appear at t=1.3T and develop fully by t=5.3T. For t>5.3T, the wave packets continue to propagate with only some regions undergoing interference. The structure of the pressure field reveals that some regions are free of interference, where the wave packets propagate independently from each other. Interestingly, the mesh-like region of interference is observed to propagate along a 45° diagonal. For t>7.9T, some afterwaves are observed by the LDV, again resulting from the loudspeakers mechanical inertia. As with the reflection experiment, there is good spatial and temporal agreement between FE simulation and LDV (Figure 7).

4.4 FEA simulation of reflection and interference

Reflection and interference were simulated using a time-dependent acoustic pressure model. A 2D air domain of 300mm x 300mm with 15 quadratic triangular elements per wavelength was used. A mesh convergence study was carried out, showing that 6 elements/wavelength would be sufficient to represent the sound field. Yet, at low computational cost, 15 elements were used to match the experimental spatial

resolution. The models included an acoustic source boundary to simulate the loudspeaker(s), a sound radiation boundary to simulate the waves propagating out of the model space, and a sound hard boundary to simulate a reflecting surface. The number of elements used was 45k for reflection and 48k for the interference experiments. Results of both simulations are shown in Figure 7. As with most loudspeakers, producing a finite wave packet is difficult to achieve due to the mechanical inertia of the sound radiating elements, therefore some differences in the experimental and FEA results are expected for the trailing edge of the wave packet.

4.5 Critical evaluation of the method

To verify the quantitative validity of the method, the acoustic pressure measured by LDV was compared to that of the reference microphone. LDV time-resolved signal was taken from a measurement point 1mm away from the microphone (Figure 8). This comparison corroborates previous reports that laser interferometry can be used to infer pressure from refractive index modulation [13] [29]. There is good agreement between microphone and calculated LDV pressure, both in magnitude and phase (Figure 8). Some differences exist between the two signals that are not fully understood. A key difference resides in the fact that the precision microphone detects pressure changes in all three spatial directions, whereas the LDV measurement reports pressure changes along the direction of the laser path, the integration line. In addition, the microphone is detecting sound pressure over a region of air, of unknown volume and geometry. It may therefore be possible that LDV integration done at 1 mm distance does not reflect in detail the pressure integrated by the pressure microphone. Interestingly, technical information on the actual acoustic sampling of microphones does not provide the spatial details necessary to resolve this issue. The technique presented here, applied with an increased scanning resolution, may be useful to perform such analysis.

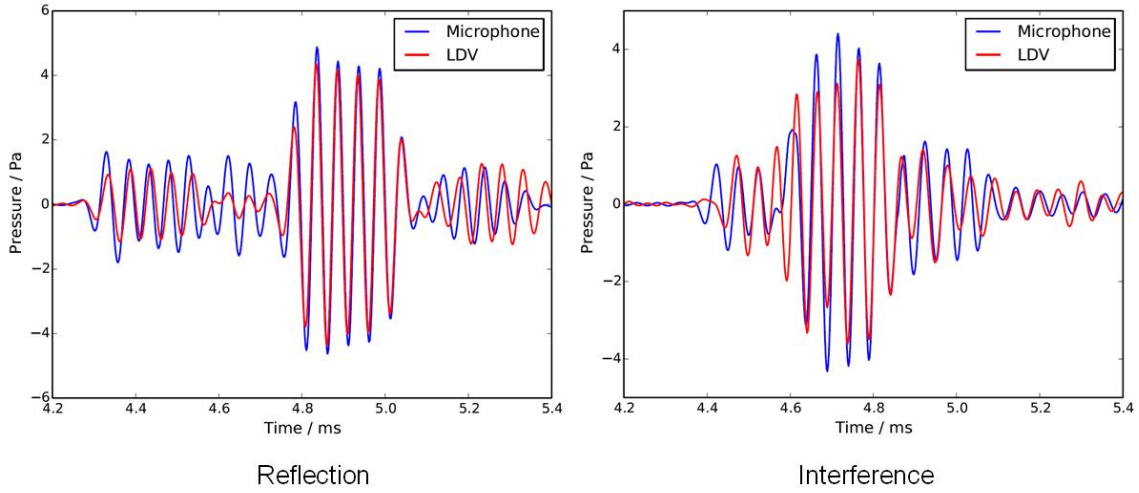

Figure 8 – Comparison of sound pressure for reference microphone and LDV pressure measurements. LDV point taken 1mm from microphone tip.

5 Discussion

We have shown that a quantitative spatial and temporal reconstruction of 2D acoustic waves can be achieved by way of laser Doppler vibrometry and simple transformation of the velocity signal. The study shows that the geometry of the sound source is an important factor to consider regarding the accuracy of quantified reconstruction of acoustic fields. The measurement error introduced by non-parallel scanning lines can be reduced by a conjunction of three methodological adjustments; the use of a planar loudspeaker with narrow beam width, a sufficiently large laser-reflector distance and suitably large wavelengths. The use of a telecentric lens in the LDV would contribute to the optimisation and flexibility of the technique.

The FEA data and analysis (Figure 5) suggest that the effective acoustic beam width of the point source is highly scattered for the frequencies considered. From Figure 4-A it is apparent that multiple points along the integration line contribute to the average signal. The present analysis shows that the quantification of sound pressure radiating from a point source is ambiguous. While the sound field can be visualised, a quantitative approach appears not to be practical at the moment. For the planar source, however, a calculated estimate of the beam width is possible. Whilst the spatial scatter of the beam width, *a,* for the point source is large irrespective of frequency (Figure 5), the planar source yields values of *a* with a clear structure for frequencies >5kHz. Surface reflection and interference have been accurately reconstructed in terms of spatial organisation, magnitude and phase. FEA corroborates the experimental field visualisation, providing a good match to LDV measurement (Figure 7). The refracto-vibrometry method also accurately reports on sound pressure level, as confirmed by comparison to a reference precision microphone (Figure 8). Knowledge of *a* is required for a correct calculation of the average sound pressure within the observable pressure field. The exact shape of this field is dependant upon the geometry of the acoustic radiators and the acoustic interactions with nearby structures. A consequence being that the effective value of *a* may be difficult to estimate, thereby precluding quantification.

We also suggest that the variable value of *a* dependant upon the scanning direction, Figure 3, and radiator/reflector orientation will have an effect on the quantitative resolution of 3D CT reconstructions as the transforms used for the reconstructions assume the scanned domain to be insensitive to scanning direction. As a result of the error analysis in this study, the feasibility of quantitative 3D CT reconstructions requires further consideration.

6 Conclusions

The visualisation of sound fields is rarely used as a diagnostic or analytical tool in acoustic research, industrial noise analysis or product development. Refracto-vibrometry is shown to be a rapid, accurate method that can lend itself to research and industrial applications. The present analysis shows that by carefully considering the geometry of the sound radiator, it is possible to produce accurate sound field imaging. The method presented here does not require extensive calculations and unwarranted

assumptions, and therefore could find practical uses. While some limitations still exist, scanning refracto-vibrometry holds the promise of improving the non-contact, clutter-free quantitative evaluation of acoustic fields.

7 Acknowledgments

This research is part of a research programme on the mechanics of auditory systems funded by the BBSRC. DR acknowledges support from the Royal Society of London. The authors also kind thank Dr. Milena Martarelli for the fruitful discussions regarding CT reconstructions.

8 References

[1] H. Kleine, H. Grönig, K. Takayama, Simultaneous Shadow, Schlieren and Interferometric Visualization of Compressible Flows, Optics and Lasers in Engineering. 44 (2006) 170–189.

[2] P.A. Chinnery, The schlieren image of two-dimensional ultrasonic fields and cavity resonances, The Journal of the Acoustical Society of America. 101 (1997) 250–256.

[3] W. Merzkirch, Flow Visualization, 2nd ed., Academic Press Inc, London, 1987.

[4] T.A. Pitts, J.F. Greenleaf, Three-dimensional optical measurement of instantaneous pressure., The Journal of the Acoustical Society of America. 108 (2000) 2873–83.

[5] K. Nakamura, Sound field measurement through the acousto-optic effect of air by using laser Doppler velocimeter, in: 4th Pacific Rim Conference on Lasers and Electro-Optics, IEEE, Chiba-Japan, 2001: pp. 154–155.

[6] L. Zipser, H. Franke, E. Olsson, N.E. Molin, M. Sjödahl, Reconstructing two-dimensional acoustic object fields by use of digital phase conjugation of scanning laser vibrometry recordings., Applied Optics. 42 (2003) 5831–5838.

[7] C. Vuye, S. Vanlanduit, P. Guillaume, Accurate estimation of normal incidence absorption coefficients with confidence intervals using a scanning laser Doppler vibrometer, Optics and Lasers in Engineering. 47 (2009) 644–650.

[8] X. Jia, G. Quentin, M. Lassoued, Optical heterodyne detection of pulsed ultrasonic pressures., IEEE Transactions on Ultrasonics, Ferroelectrics, and Frequency Control. 40 (1993) 67–9.

[9] E. Olsson, K. Tatar, Sound field determination and projection effects using laser vibrometry, Measurement Science and Technology. 17 (2006) 2843–2851.

[10] L. Zipser, H. Franke, Refracto-Vibrometry for Visualizing Ultrasound in Gases, Fluids and Condensed Matter, in: 2007 IEEE Ultrasonics Symposium Proceedings, IEEE, 2007: pp. 395–398.

[11] N. Paone, G.M. Revel, Modelling and experimental analysis of the performance of a laser Doppler vibrometer used to measure vibrations through combustive flows, Optics and Lasers in Engineering. 30 (1998) 163–178.

[12] P. Castellini, M. Martarelli, Aeroacoustic characterization of turbulent free jets using scanning laser Doppler vibrometry, in: Sixth International Conference on Vibration Measurements by Laser Techniques: Advances and Applications, Ancona-Italy, 2004: pp. 215–224.

[13] A. Torras-Rosell, S. Barrera-Figueroa, F. Jacobsen, Sound field reconstruction using acousto-optic tomography., The Journal of the Acoustical Society of America. 131 (2012) 3786–93.

[14] M. Martarelli, P. Castellini, E.P. Tomasini, Subsonic jet pressure fluctuation characterization by tomographic laser interferometry, Experiments in Fluids. 54 (2013) 1626.

[15] G.M. Revel, G. Pandarese, A. Cavuto, Quantitative validation of an air-coupled ultrasonic probe model by Interferometric laser tomography, in: 10th International Conference on Vibration Measurement by Laser and Non-Contact Techniques, Ancona-Italy, 2012: pp. 361–369.

[16] P. Castellini, M. Martarelli, Uncertainty Analysis of Hybrid Numerical-Experimental Procedures: Application to Flow Density Measurements, in: IMAC XXIV, Conference & Exposition on Structural Dynamics, St Louis-USA, 2006: p. 9.

[17] M. Martarelli, P. Castellini, E.P. Tomasini, Coherent Tomographic Laser Interferometry for the aero-acoustic characterization of cold jets, in: 16th International Symposium on Applied Laser Techniques to Fluid Mechanics, Lisbon-Portugal, 2012.

[18] R. Wimberger-Friedl, The assessment of orientation, stress and density distributions in injection-molded amorphous polymers by optical techniques, Progress in Polymer Science. 20 (1995) 369–401.

[19] R.M. Waxler, W.C. E, Effect of Hydrostatic Pressure on the Refractive Indices of Some Solids, Journal of Research of the National Bureau of Standards -A. 69A (1965) 325–333.

[20] B. Edlén, The Refractive Index of Air, Metrologia. 2 (1966) 71–80.

[21] Y. Oikawa, Sound Field Measurements Based on Reconstruction from Laser Projections, in: IEEE International Conference on Acoustics, Speech, and Signal Processing, IEEE, Philadelphia-USA, 2005: pp. 661–664.

[22] L. Zipser, H.-D. Seelig, H. Franke, Refracto-vibrometry for visualizing ultrasound in small-sized channels, cavities and objects, in: International Ultrasonics Symposium, Rome-Italy, 2009: pp. 2588–2591.

[23] E. Olsson, Three-dimensional selective imaging of sound sources, Optical Engineering. 48 (2009) 035801.

[24] Y. Wang, P. Theobald, J. Tyrer, P. Lepper, The application of scanning vibrometer in mapping ultrasound fields, Journal of Physics: Conference Series. 1 (2004) 167–173.

[25] K. Nakamura, M. Hirayama, S. Ueha, Measurements of air-borne ultrasound by detecting the modulation in optical refractive index of air, in: IEEE Ultrasonics Symposium, Munich-Germany, 2002: pp. 609–612.

[26] A. Dittmar, R. Behrendt, Measuring the 3D propagation of sound waves using scanning laser vibrometry, in: Berlin Beamforming Conference, berlin, 2008.

[27] E. Olsson, Selective imaging of sound sources in air using phase-calibrated multiwavelength digital holographic reconstructions, Optical Engineering. 46 (2007) 075801.

[28] I. Solodov, D. Döring, G. Busse, Air-coupled laser vibrometry: analysis and applications, Applied Optics. 48 (2008) 33–37.

[29] R. Balek, Z. Slegrova, A Comparison of Acoustic Field Measurement by a Microphone and by an Optical Interferometric Probe, Acta Polytechnica. 42 (2002) 13–17.